

<https://doi.org/10.1038/s42004-025-01509-y>

# Implications of high-pressure oxygen hydrates on radiolytic oxygen in Jovian icy moons

Check for updates

Mungo Frost<sup>1,6</sup>✉, Mikhail A. Kuzovnikov<sup>2,6</sup>, Philip Dalladay-Simpson<sup>3</sup>, Ross T. Howie<sup>2,3</sup>, John S. Loveday<sup>2</sup>, Umbertoluca Ranieri<sup>2</sup> & Eugene Gregoryanz<sup>2,4,5</sup>✉

Various icy moons, such as Europa and Ganymede, have thin oxygen atmospheres and exhibit spectral features attributed to oxygen held in their surface ices. The oxygen forms from the radiolysis of water. The interiors of these bodies are subject to high pressures and it is not known how deep into icy moons oxygen-bearing ices can penetrate, or the structures formed by the oxygen–water system at high pressure. Here, we show that oxygen hydrates are stable to 2.6 GPa, allowing them to penetrate deep into icy moons, both above and below proposed sub-surface liquid-water oceans. Similarities between oxygen and hydrogen hydrates indicate potentially enhanced recombination rates, transforming them back into water and offering a resolution to the discrepancy between predicted and measured radiolysis rates. In addition to the low-pressure CS-II clathrate, our results find three high-pressure phases in the oxygen–water system: an ST clathrate, a C<sub>0</sub> hydrate, and a filled ice isomorphous with methane hydrate III. This shows a vast storage potential for molecular oxygen in icy moons and indicates that Europa could still be absorbing oxygen into its crustal ice.

Oxygen-containing atmospheres have been observed on various icy moons in the solar system, including the Jovian moons Europa and Ganymede<sup>1–3</sup>. This oxygen arises from the radiolysis of the water by high-energy radiation incident on their icy surfaces<sup>4</sup>. The radiation converts water into oxygen and hydrogen with the lighter hydrogen being preferentially lost into space, resulting in atmospheres enriched in oxygen. Models of radiolytic oxygen production rates extend over two orders of magnitude<sup>5–7</sup>, while very recent direct measurement of the hydrogen loss rate on Europa by the Juno probe places the net oxygen production rate at  $12 \pm 6 \text{ kg s}^{-1}$ , compatible with only the lowest of modelled rates<sup>8</sup>.

Understanding of the fate of the radiolytic oxygen is hampered by uncertainty in the water ice–oxygen interaction. Spectra taken from the surface of Ganymede have an absorption feature that is attributed to a simultaneous transition in adjacent oxygen molecules, and which is of far higher intensity than can arise from atmospheric density<sup>7</sup>. The temperature on the surface is above the boiling point of oxygen, so it has been suggested that this feature arises from a high density of oxygen in the surface ice of the moon<sup>2,3</sup>.

At low pressure ( $P$ ) and low temperature ( $T$ ), oxygen is known to be absorbed into a modified ice structure called a gas clathrate<sup>9,10</sup>. Gas clathrate hydrates are a class of inclusion compounds in which small molecules are held within cages formed from hydrogen-bonded water molecules<sup>11</sup>. More generally, gas hydrates include both clathrates and other host-guest compounds where guest species occupy open channels in a host water lattice. The application of pressure usually stabilizes these compounds to higher temperatures and can induce phase transitions between different host–guest configurations<sup>12</sup>. Clathrates adopt a number of phases, with two cubic structures, CS-I and CS-II, which are commonly observed at low pressure, and tetragonal, ST, or hexagonal, SH, modifications which are more common at higher pressure<sup>12,13</sup>. At high pressures, of the order of a few GPa, many small molecules form “filled ice structures” in which the guest molecules are held within voids in modified ice lattices<sup>14–17</sup>.

Neutron diffraction studies on the low- $PT$  oxygen clathrate found it to adopt the CS-II clathrate structure with  $a = 17.253 \text{ \AA}$ <sup>18,19</sup>. The CS-II clathrate structure has two distinct types of cage with 16 smaller dodecahedral (12-faced) cages, and 8 larger hexakaidecahedral (16-faced) cages in the unit cell.

<sup>1</sup>High Energy Density Sciences Division, SLAC National Accelerator Laboratory, 2575 Sand Hill Road, Menlo Park, CA, 94025, USA. <sup>2</sup>Centre for Science at Extreme Conditions, University of Edinburgh, King's Buildings, Edinburgh, EH9 3FD, UK. <sup>3</sup>Center for High Pressure Science and Technology Advanced Research, 1690 Cailun Road, 201203 Shanghai, China. <sup>4</sup>SHARPS (Shanghai Advanced Research in Physical Sciences), 68 Huatuo Rd, Bldg 3, 201203 Pudong, Shanghai, China. <sup>5</sup>Key Laboratory of Materials Physics, Institute of Solid State Physics, HFIPS, Chinese Academy of Sciences, 230031 Hefei, China. <sup>6</sup>These authors contributed equally: Mungo Frost, Mikhail A. Kuzovnikov. ✉e-mail: [mdfrost@slac.stanford.edu](mailto:mdfrost@slac.stanford.edu); [e.gregoryanz@ed.ac.uk](mailto:e.gregoryanz@ed.ac.uk)

The formation of the CS-II structure is attributed to the oxygen molecule fitting favorably in both the smaller and larger cage types<sup>18</sup>.

The effect of pressure on oxygen clathrate, and the oxygen–water system in general, has not previously been studied. The  $P$ – $T$  stability of oxygen clathrate determines how deep within the moons it can penetrate and therefore affects their possible internal compositions. An internal source of molecular oxygen would lead to drastically different chemical processes within oxygen-rich icy moons, such as Europa and Ganymede, compared to methane-rich ones, such as Titan<sup>14,20,21</sup>.

In this study, we investigate the oxygen–water system over a range of pressures and temperatures relevant to the interiors of icy moons using diamond anvil cells probed by synchrotron powder x-ray diffraction and Raman spectroscopy. This reveals oxygen hydrates to be stable to 2.6 GPa at ambient temperature and suggests that oxygen-bearing ices can penetrate deep into icy moons. In addition to the known CS-II structure oxygen clathrate, upon compression, we also find an ST clathrate, a  $C_0$  structure hydrate, and a filled ice isostructural with methane hydrate III (MH-III), prior to decomposition into oxygen and ice VII at 2.6 GPa. The high-pressure stability of oxygen hydrates opens the potential for large quantities of molecular oxygen to be hosted within icy moons with implications for their internal composition, chemistry, and habitability. Similarities between the clathrate hydrates of  $O_2$  and  $H_2$  suggest that the surface ices may preferentially hold them in close proximity. This offers a mechanism by which their recombination rate can be enhanced and may explain the disagreement between theoretical<sup>5–7</sup> and measured<sup>8</sup> rates of water radiolysis.

We also extend the pressure dependence of the decomposition temperature to 1.1 GPa, revealing the CS-II clathrate to be stable in a region of the phase diagram where water is liquid. Compression at 66 K yields a clathrate with a Raman spectrum compatible with the CS-II structure up to

1.44 GPa, above which the peaks broaden, likely due to the collapse of the open cage structure. The ambient-temperature phase transitions also exhibit large pressure hysteresis and some variability between experiments, depending on the compression rate. This is attributed to kinetic hindrance in the transitions, which, coupled with the narrow stability fields of the ST and  $C_0$  phases, can result in their being bypassed. Faster compression can result in premature decomposition of the clathrates into separate ice VI or VII and oxygen.

## Results

Figures 1 and 2 show the pressure evolution of the Raman spectra of the oxygen–water system. At low pressure, the vibrational Raman feature of the enclathrated  $O_2$  consists of three peaks, the positions of which are insensitive to pressure. At around 1.0 GPa these transform into a single narrow peak which moves to higher shift and broadens above 1.2 GPa. The broader peak moves to a higher shift with increasing pressure before undergoing a further transition to a narrow peak at a higher shift at 1.6 GPa. This peak is still softer than that arising from free  $O_2$  and hardens with pressure up to 2.6 GPa above which only the  $O_2$  stretch of free oxygen remains.

Oxygen clathrate forms at ambient temperature at 0.16(5) GPa, in agreement with the low- $PT$  decomposition curve<sup>9</sup>. Powder x-ray diffraction (XRD), Fig. 3a, reveals the low-pressure phase to have the CS-II structure (space group  $Fd\bar{3}m$ ) previously observed for oxygen clathrate at low  $PT$ <sup>8,19</sup>. At 0.22 GPa it has lattice parameter  $a = 17.183(4)$  Å. This corresponds to the pressure range where multiple  $O_2$  stretching Raman peaks are observed. The three vibrational modes arising from  $O_2$  (see Figs. 1 and 2), are softer than that of pure oxygen and their positions are insensitive to pressure. On an intensity basis the lowest frequency one, at  $1548\text{ cm}^{-1}$  is attributed to oxygen molecules in the smaller cage, while the higher frequency pair, at 1550 and

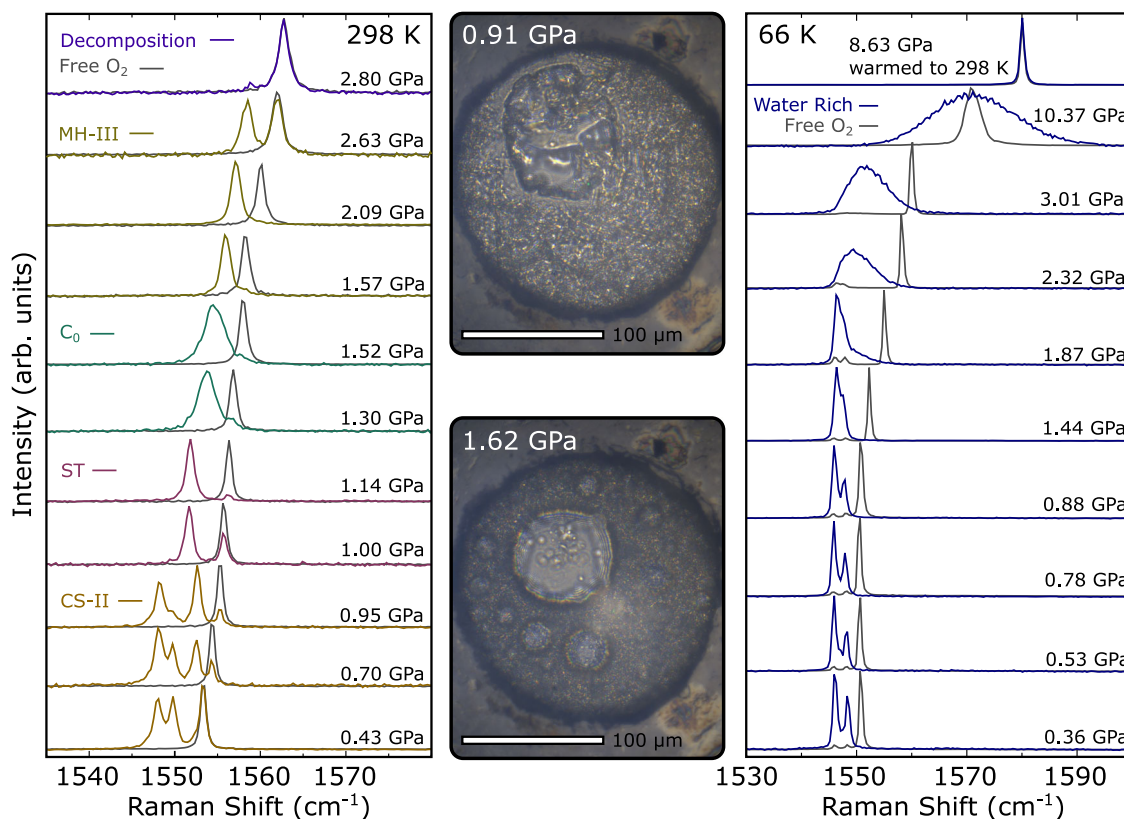


**Fig. 1 | Raman spectra of the  $O_2$  vibrational mode at selected pressures.** Spectra were collected on both the water-rich part of the sample and on the excess free oxygen. *Left:* At 298 K. Spectra of excess free oxygen in gray, spectra of hydrate phases colored according to the phase attributed to each of them based on the number, position, and width of the  $O_2$  vibrational Raman feature(s) (see also Fig. 2). *Right:* At 66 K.

Enclathrated oxygen in navy and free oxygen in gray. Below 1.44 GPa this is consistent with a CS-II clathrate, above this, the host water lattice appears to collapse. On warming at 8.63 GPa, only free oxygen is observed. *Center:* Photographs of a sample in the CS-II phase with embedded excess oxygen at 0.91 GPa then after decomposition due to fast compression to 1.62 GPa showing separate oxygen and ice VII phases.

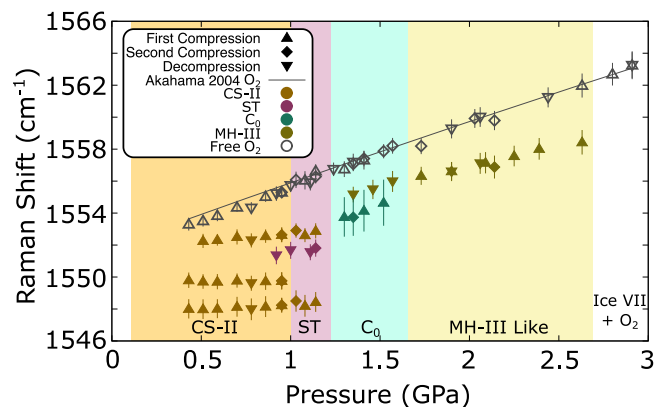


**Fig. 2 | Oxygen vibrational band frequencies and full widths at half maxima (FWHM) vs pressure.** Symbols represent Raman frequencies measured in our study. The symbol shapes refer to the stage of the experiment and their colors to the assigned phase. The bars indicate the FWHM of the oxygen vibrational Raman feature(s). The stability fields of different phases overlap and transition pressures are the best estimates. Note the broader Raman feature of the  $C_0$  phase. The grey line is the pure oxygen vibrational frequency<sup>61</sup> with the corresponding peak arising from excess free molecular oxygen in the sample.

1552  $\text{cm}^{-1}$ , arise from the larger cages with single and multiple occupancies respectively. On increasing pressure, intensity is moved from the peak at 1550  $\text{cm}^{-1}$  to the one at 1552  $\text{cm}^{-1}$ . The guest molecular stretching Raman mode of CS-II hydrogen clathrate exhibits similar characteristics with three hydrogen environments corresponding to the smaller cage and singly and multiply occupied larger cages in order of increasing frequency<sup>22</sup>. Rietveld refinement of the cage occupancies supports this interpretation finding that the occupancy of the larger cages increases with pressure, from 1  $\text{O}_2/\text{cage}$  at 0.2 GPa to 2.8  $\text{O}_2/\text{cage}$  at 1.4 GPa.  $\text{O}_2/\text{H}_2\text{O}$  content for the small and large cages of the CS-II phase, as well as for the other phases is shown in Fig. 4.

Above about 1 GPa, the multiple  $\text{O}_2$  stretching Raman peaks of the CS-II phase are replaced by a single one. Based on x-ray diffraction, Fig. 3b, this is attributed to a structural transformation to ST structure oxygen clathrate. On compression, this transition is easily overdriven resulting in the omission of this phase, though it is usually observed on decompression. This likely arises from metastability leading to a hysteresis in its formation pressure which is similar to or greater than the width of its narrow pressure stability field. The ST phase has a single narrow Raman feature arising from the enclathrated  $\text{O}_2$  molecules, which is softer than that of pure oxygen (see Figs. 1 and 2). This is expected as the host lattice consists of a single cage type. The ST structure is also observed in the argon–water and nitrogen–water systems<sup>17,23,24</sup>. It is tetragonal with space group  $P4_2/mnm$  and ST oxygen clathrate has lattice parameters  $a = 6.298(1) \text{ \AA}$ ,  $c = 10.703(2) \text{ \AA}$  at 1.44 GPa. Rietveld refinement of the powder x-ray diffraction pattern of ST oxygen clathrate at 1.44 GPa is shown in Fig. 3 and reveals the occupancy of the single cage type to be close to 1.6  $\text{O}_2/\text{cage}$ .

Between 1.2 and 1.6 GPa powder x-ray diffraction reveals a further structural modification forming  $C_0$  structure oxygen hydrate. After this transition, the narrow  $\text{O}_2$  stretch Raman peak of the ST phase, the frequency of which is insensitive to pressure, broadens and moves to higher frequency on compression, see Fig. 2.  $C_0$  hydrates have a chiral structure in which the guest species occupy open channels in a water network that is unrelated to any stable ice phase.  $C_0$  oxygen hydrate has the trigonal space group  $P3_112$  and  $a = 6.218(2) \text{ \AA}$  and  $c = 6.273(4) \text{ \AA}$  at 1.82 GPa, x-ray diffraction data are presented in Fig. 3c. The same structure has previously been observed in the hydrogen–water and  $\text{CO}_2$ –water systems<sup>25,26</sup>.  $C_0$  oxygen hydrate has also previously been formed by refilling an empty  $C_0$  structure at low  $PT$ <sup>27</sup>. Like the ST clathrate, this structure has only one environment for the guest oxygen and it has a single broad vibrational mode, shown in Figs. 1 and 2. The greater width of this feature in the  $C_0$  phase may arise from the anisotropy in the local environment for the guest oxygen molecules or from the

fact that the molecules may be mobile in the channels as they appear to be in carbon dioxide and hydrogen hydrates with the  $C_0$  structure<sup>26</sup>.

Above 1.6 GPa the  $\text{O}_2$  stretching Raman peak narrows and hardens. X-ray diffraction, Fig. 3d, reveals this to arise from a phase transformation of the  $C_0$  phase into a filled ice which is isomorphous with methane hydrate III. In this phase, the oxygen guest molecules occupy channels in a modified ice structure that closely resembles ice  $Ih$ <sup>12,14,28</sup>. Like the  $C_0$  and ST phases, it has a single environment for the guest molecules, and correspondingly has a single Raman peak arising from  $\text{O}_2$  molecular vibrations. This is narrower and slightly harder than that of the  $C_0$  phase, distinguishing their Raman spectra. The MH-III phase's  $\text{O}_2$  vibrational mode hardens with pressure but remains softer than that of pure oxygen. It is the densest of the oxygen-hydrate phases with the highest  $\text{O}_2$  content (see Fig. 4), and has the orthorhombic space group  $Imma$  and  $a = 8.034(2)$ ,  $b = 4.678(1)$ , and  $c = 7.706(2) \text{ \AA}$  at 2.34 GPa.

Above 2.6 GPa, MH-III structure oxygen hydrate decomposes into separate oxygen and ice VII phases, as evidenced by the absence of any hydrate phases in x-ray diffraction patterns and the only  $\text{O}_2$  vibrational Raman feature corresponding to that of free oxygen. Argon forms a similar filled ice which decomposes above 6.0 GPa<sup>15</sup>, however, the filled ices of hydrogen and methane are stable to much higher pressures<sup>12,29</sup> making the decomposition pressure of oxygen hydrate unusually low.

The low-temperature behavior of the oxygen–water system on compression was studied at 66 K, representative of the surfaces of Jovian moons, using Raman spectroscopy. Below 1.44 GPa, the oxygen vibrational Raman feature is a doublet and softer than that of pure oxygen (see Fig. 1) This is assigned to the CS-II clathrate, in agreement with low-temperature and low-pressure neutron studies<sup>18,19</sup>. The peaks are resolved up to 1.87 GPa, above which the feature becomes extremely broad and more symmetric with pressure and hardens until it is centered at the same position as pure oxygen by 10.37 GPa. This likely arises from the pressure-induced collapse and amorphization of the oxygen clathrate. Pressure-induced amorphization of low-temperature water ice is well known<sup>30</sup> and clathrate hydrates of various gases have been shown to behave similarly<sup>31</sup>. The O–H stretch feature also broadens on compression at 66 K (see Supplementary Figs. S2 and S3), apparently without the formation of ice VIII<sup>32</sup>, supporting this interpretation. Warming to 298 K near 10 GPa recovers separate oxygen and ice VII as expected.

On heating, oxygen clathrate is observed to decompose at lower temperatures than many other gas clathrates<sup>12,33–35</sup>. The decomposition curve was measured to 1.1 GPa and is shown in Fig. 5. Cooling the dissociated mixture of fluid water and oxygen below 1.1 GPa reversibly causes the CS-II clathrate to form, however above this pressure separate ice VI and oxygen survive metastably, which hindered our efforts to extend the decomposition curve to higher pressure.

## Discussion

The CS-II clathrate has three vibrational modes arising from the  $\text{O}_2$  guest molecules (see Figs. 1 and 2), despite the structure comprising only two types of cage. This arises from the differing occupancy of the larger cage. Multiple cage occupancy also occurs in the CS-II clathrate hydrates of other gases, such as helium<sup>36</sup> and hydrogen<sup>37,38</sup>. With pressure increase, intensity is lost from the central peak, corresponding to singly occupied large cages, and increases in the highest frequency one, indicating that the population of multiply occupied cages increases with pressure. Rietveld refinement of the cage occupancy agrees with this interpretation, as shown in Fig. 4. The smaller cages are found to have an average occupancy of 0.85  $\text{O}_2/\text{cage}$  which is insensitive to pressure and close to the value found by neutron diffraction at low pressure<sup>18</sup>. In contrast to this, the occupancy of the large cages is found to increase with pressure reaching a maximum of 2.8  $\text{O}_2$  per cage at maximum pressure.

MH-III structure oxygen hydrate decomposes at 2.6 GPa at room temperature. This is low compared to other gas hydrates. Nitrogen and argon hydrates persist to several GPa<sup>12,29</sup>, and hydrogen<sup>39</sup> and methane<sup>40</sup> hydrates to at least 90 and 150 GPa, respectively. It is also interesting to

**Fig. 3 | Powder diffraction patterns of oxygen hydrate phases.** Panels show integrated powder x-ray diffraction patterns of the oxygen–water system (upper black trace) with Rietveld fits (colored trace) and residuals (lower black trace), ticks indicate allowed peak positions by phase. **a** CS-II clathrate at 0.22 GPa. **b** ST clathrate at 1.44 GPa. **c** C<sub>0</sub> hydrate at 1.82 GPa. **d** MH-III-like structure filled ice and ice VII at 2.34 GPa. Inset images show host cages. Refer to the text for uncertainties in lattice parameters, structural details are presented in Supplementary Note I.

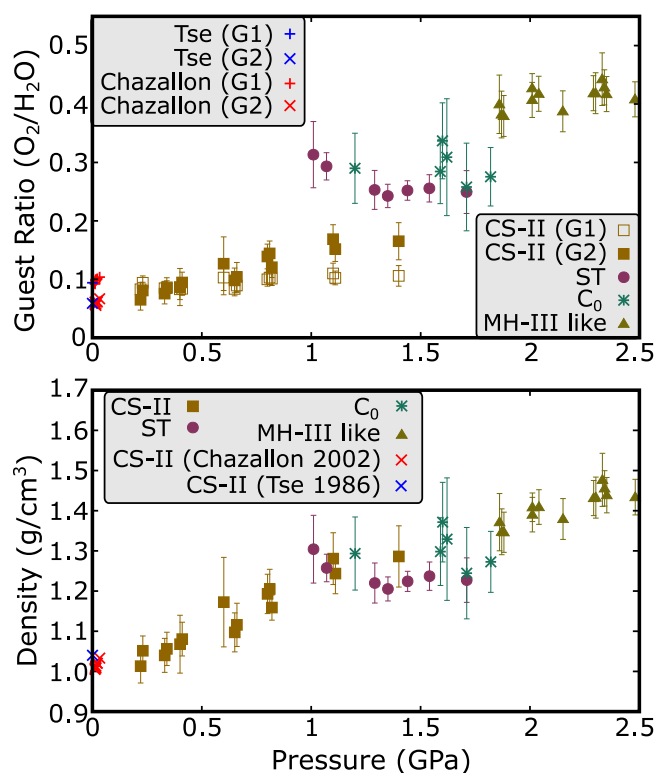
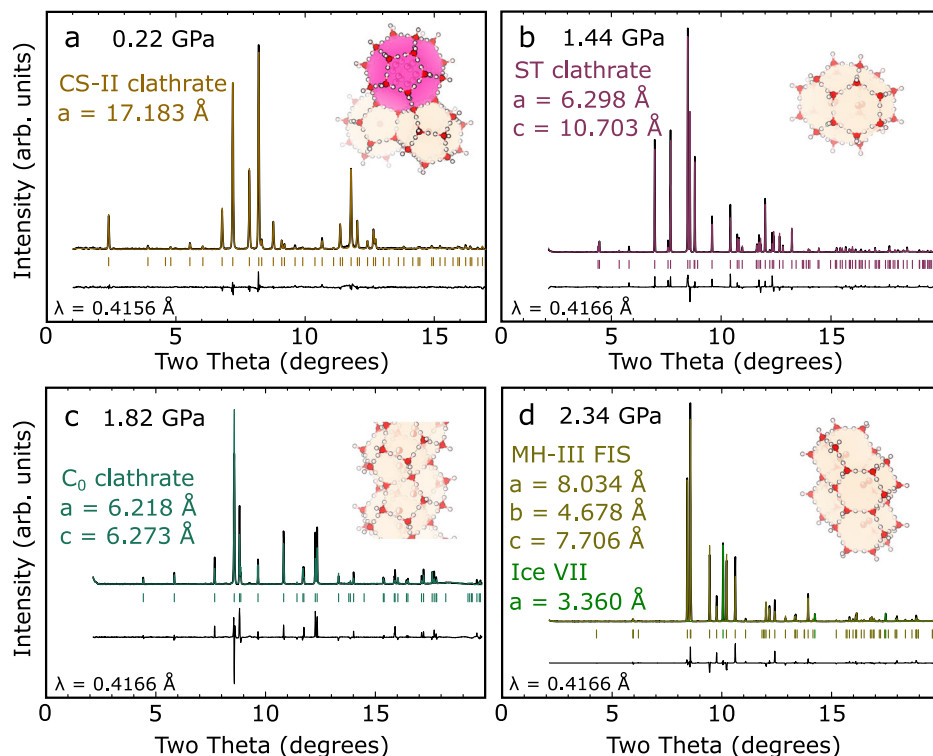


**Fig. 4 | O<sub>2</sub> content and density of oxygen hydrates vs pressure.** *Top:* Molar ratio of O<sub>2</sub> guest per H<sub>2</sub>O molecule in the water lattices. Occupancy is based on Rietveld refinement. ‘G1’ is the smaller of the two CS-II cages and ‘G2’ the larger, with the total oxygen concentration being their sum. Literature points on the CS-II clathrate are from Chazallon et al.<sup>19</sup> in red and Tse et al.<sup>18</sup> in blue. *Bottom:* Density of oxygen hydrates vs pressure. Uncertainty in density mainly arises from uncertainty in guest occupancy. Error bars are one standard deviation. Volume per water molecule and *c/a* ratios are reported in the Supplementary Fig. S1.

compare the hydrate clathrates of oxygen and nitrogen as both are small diatomic molecules with kinetic diameters of 3.46 and 3.64 Å respectively<sup>41</sup>. At low pressures both adopt the CS-II clathrate structure, presumably due to their similar sizes, however on compression they show marked differences. As shown above, at ambient temperature oxygen hydrate follows the transition series from CS-II to ST to C<sub>0</sub> to MH-III before decomposition. In contrast to this, nitrogen transforms from the CS-II to SH structure at 0.9 GPa followed by a transition to the ST structure at 1.6 GPa then forms a filled ice at 2 GPa which remains stable to at least 30 GPa<sup>12,17</sup>. Given their similar molecular sizes, these differences in the high-pressure behaviors of oxygen and nitrogen hydrate likely arise from the smaller molecular volume of fluid oxygen at this pressure. The unit cell volumes of the MH-III phase are similar for both species, however, the volume of compressed fluid nitrogen around 2 GPa is substantially higher than that of oxygen<sup>42,43</sup> which stabilizes MH-III-like nitrogen-filled ice to a higher pressure than that of oxygen.

Oxygen has been detected in spectra taken from the surface of Ganymede, where it is likely held in the form of a low-pressure clathrate<sup>2</sup>, and oxygen clathrates have been suggested to be a component of subsurface ices in Europa<sup>3</sup>. The results here suggest that oxygen can be incorporated deep into icy moons, and could have a substantial effect on their internal chemistry, with oxygen-bearing ices stable both above and below the proposed subsurface liquid water oceans<sup>44–46</sup>. While the limited pressure and thermal stability of oxygen hydrate impede its penetration to the core regions of larger icy moons, smaller ones such as Europa have much lower pressures within them, below 1 GPa. The increased thermal stability of CS-II oxygen hydrate with modest pressure increase, Fig. 5, implies that oxygen hydrate could exist deep within the European ices.

Oxygen hydrates were studied at temperatures from 66 K to their decomposition at around 306 K. Such temperatures are representative of icy moons. For example, the surface of Europa varies from 50 K in the polar regions to around 100 K near the equator<sup>47</sup>, while its interior is believed to be warmer and contains liquid water<sup>47</sup>. Liquid water ‘oceans’ have been proposed in the interiors of several icy moons<sup>44–46</sup> which can have higher internal temperatures due to tidal heating. Liquid water, and other small molecules, have been observed to be ejected from their interiors to the

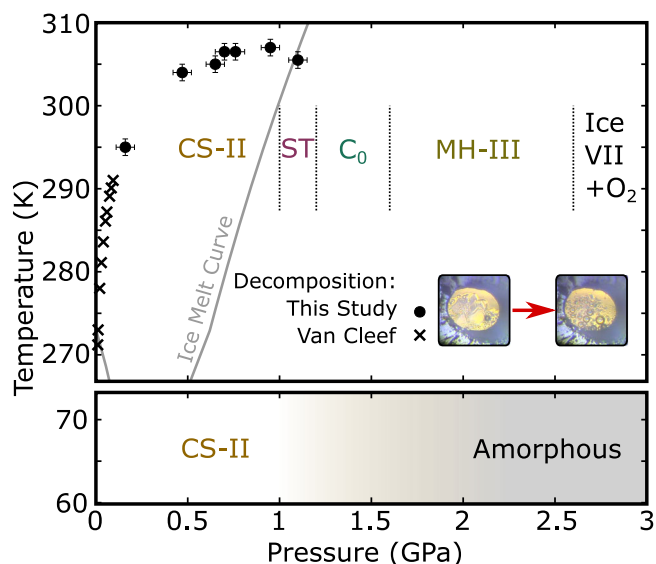


**Fig. 5 | Summary of the phases observed in the oxygen–water system.** The decomposition curve of CS-II oxygen clathrate is shown with one sigma error bar. The gray line shows the melt curve of ice<sup>62</sup>. CS-II oxygen clathrate is stable to higher temperatures than ice VI. Insets show photographs of the sample before (left) and after (right) thermal decomposition showing bubbles of O<sub>2</sub> sinking in liquid water with 200  $\mu\text{m}$  field of view. Crosses at low pressure are decomposition data from Van Cleef et al.<sup>9,10</sup>. Amorphization at 66 K occurs between 1.4 and 2.3 GPa, indicated by the shaded region.

surface in the process of cryovolcanism<sup>48–50</sup>. Where the ejected material is retained by the moon's gravity it will freeze on the cold surface burying the material previously there. This provides a mechanism for the transport of surface material, including oxygen hydrate, deeper into the interior ice and allows oxygen to permeate deeper than the surface radiolytic processes can reach.

Oxygen and hydrogen share some structural motifs in their high-pressure hydrates with both forming CS-II and C<sub>0</sub> phases. The CS-II phase exhibits multiple cage occupancy with both guest species<sup>37</sup> and may explain the substantially higher oxygen formation rate predicted on Europa compared to the value measured by the Juno probe<sup>5–8</sup>. The oxygen is produced by radiolysis of water by high energy charged particles from Jupiter's magnetospheric plasma. These will penetrate the ice to some degree with the result that the oxygen and hydrogen are created within the first meter of ice<sup>51</sup>. Both species form CS-II clathrates so if the mixture also does<sup>52</sup>, as is the case for a mixture of oxygen and nitrogen<sup>19</sup>, then some of the molecular oxygen and hydrogen will be preferentially held in close proximity by the host ices, enhancing the rate at which they react and turn back into water.

The Juno probe measured the net rate of hydrogen loss from Europa, however, the rate of radiolysis can be much higher if oxygen and hydrogen recombine while still within the surface ice. Results here suggest that Europa, and icy moons in general, have a substantial capacity to contain oxygen in their ice. It is worth noting that the oxygen production rate on Europa is inferred from the hydrogen loss rate, rather than direct measurement, and there is no observational evidence that oxygen is lost from the moon at the same rate as hydrogen<sup>8</sup>. Estimates for the thickness of the surface ice layer vary<sup>44,53</sup> but taking a value of 30 km and the oxygen content from Fig. 4, gives an estimate of the maximum O<sub>2</sub> capacity of Europa's surface ice of  $2.5 \times 10^{20}$  kg. The measured production rate by the Juno probe is  $12(6) \text{ kg s}^{-1}$ . If this rate has not substantially changed since the moon's accretion, then <1% of the capacity for the oxygen in European ice can have been filled by radiolytic O<sub>2</sub>, and its oxygen content has the potential to be increasing over geological timescales. See Supplementary Note II for details of the calculation.

Compared to other icy moons, for example, Titan, where radiolysis plays a smaller role and methane is the dominant species, this suggests distinct chemical processes occurring in different classes of the icy moon. Methane and oxygen clathrates are presumably incompatible, so icy moons with predominately methane-bearing ice interiors, like Titan, will have reducing chemistry, while those with higher oxygen contents will have oxidizing environments favoring different chemical reactions. Life developed on Earth in an anaerobic environment, so this would affect a moon's astrobiological potential<sup>54</sup>.

In conclusion, we have found several oxygen hydrate phases under pressure. The CS-II phase known at low pressure exhibits multiple occupancy of the host cages by the guest O<sub>2</sub> molecules, with a maximal occupancy of 2.8 molecules in the larger cage at the highest pressure. The CS-II clathrate transforms into the ST structure at 1.0 GPa, then into a C<sub>0</sub> phase at 1.2 GPa. Finally filled ice isomorphous with methane hydrate III forms between 1.6 and 2.6 GPa, above which it decomposes into separate oxygen and ice VII. Both oxygen and hydrogen can form CS-II clathrates and both exhibit multiple occupancy. Therefore molecular H<sub>2</sub> and O<sub>2</sub> formed by radiolysis of the surfaces of icy moons could be held in close proximity by their host water lattice leading to enhanced recombination. This presents a potential explanation for the considerably higher rate of oxygen production predicted on Europa compared to that which has been measured.

## Methods

Pressure was generated using diamond anvil cells equipped with diamonds with various culet sizes ranging from 200 to 1600  $\mu\text{m}$ . Pressure was determined from the fluorescence wavelength of a ruby chip included in each loading with an uncertainty of 0.05 GPa<sup>55</sup>. Cells were loaded with distilled or Milli-Q purified water, which was allowed to partially leak to leave room for oxygen (99.5% purity, BOC) which was subsequently loaded as a cryogenic liquid.

Raman spectra were taken using custom confocal Raman spectrometers in the backscattering geometry. Room temperature data were collected using the 647 nm line of a Kr-ion laser with a typical incident power of 10 mW focused to a  $\sim 2 \mu\text{m}$  diameter spot. The Rayleigh line was suppressed with Bragg notch filters (BragGrate, OptiGrate) and spectra were recorded with an Acton SP-2500i spectrometer equipped with a liquid nitrogen-cooled charge-coupled device (CCD). The system was calibrated with an Ar + Ne lamp between each measurement for a final resolution and spectral accuracy better than  $1 \text{ cm}^{-1}$ . Low-temperature data were collected using 532 and 660 nm excitation wavelengths focused to a spot diameter of  $2 \mu\text{m}$  and a typical incident power of 5 mW. Ultra-narrow notch filters were employed to attenuate the reflected laser light before being dispersed by an aberration-corrected spectrometer and imaged using liquid nitrogen-cooled CCD. The positions and full width at half maxima of the oxygen vibrational modes were fitted using Voigt functions in the FITYK package.

Angular-dispersive powder X-ray diffraction experiments were performed at: the ID15-b beamline at ESRF, Grenoble, France<sup>56</sup>; I15 beamline at Diamond Light Source, Didcot, UK<sup>57</sup>; and BL10XU beamline at SPring-8, Hyogo, Japan<sup>58</sup>. Typically, the cell was oscillated around  $\omega$ -axis by  $\pm 15^\circ$ , and the 2D diffraction image was collected for 20–30 s. At ID15-b an incident beam with  $E \approx 30.3 \text{ keV}$  ( $\lambda = 0.4097 \text{ \AA}$ ) was focused to about  $\sim 1 \mu\text{m}$  spot. The diffraction patterns were collected with an EIGER2 X 9M detector with a sample-to-detector distance (SDD) of 181 mm, as calibrated using a Si powder standard. At I15 we used an incident beam with  $E \approx 29.8 \text{ keV}$  ( $\lambda = 0.4156 \text{ \AA}$ ) and a MAR345 detector with an SDD of 500 mm, calibrated with a CeO<sub>2</sub> standard. At BL10XU we used an incident beam with  $E \approx 29.8 \text{ keV}$  ( $\lambda = 0.4166 \text{ \AA}$ ) with a diameter of 10  $\mu\text{m}$ , and a Perkin Elmer XRD0822 detector with SDD of 397 mm, calibrated with a CeO<sub>2</sub> standard. The SDD, detector orientation and wavelength calibration, primary processing, azimuthal integration, and background subtraction were done with the DIOPTAS v0.5.5 software<sup>59</sup>. Rietveld refinements were done with FULLPROF 7.00<sup>60</sup>.

The decomposition curve was mapped up to 1.1 GPa using cells equipped with an external resistive heater and temperature determined by a

thermocouple attached to a diamond anvil. Decomposition was determined by visual observation, where the crystalline clathrate is observed to break into immiscible water and oxygen-rich liquid phases, and by Raman spectroscopy based on the shape, position, and number of peaks from the oxygen molecular vibration, and the shape of the water O–H Raman stretching feature. Pressure was limited to the stability field of the CS-II structure clathrate due to the metastability of ice VI and fluid oxygen at higher pressure.

Low-temperature Raman measurements were carried out at 66 K using an optical dry cryostat which was cooled by liquid nitrogen. Temperatures were measured and controlled using the feedback from two Si-diodes, one placed on the cold finger and one situated on the DAC body close to the sample chamber. The pressure was manipulated at low temperatures through the inflation of a membrane with high-pressure helium gas.

### Data availability

Correspondence and requests for materials may be addressed to Mungo Frost or Eugene Gregoryanz.

Received: 24 February 2025; Accepted: 13 March 2025;

Published online: 29 April 2025

### References

- Carlson, R. et al. Hydrogen peroxide on the surface of Europa. *Science* **283**, 2062–2064 (1999).
- Spencer, J. R., Calvin, W. M. & Person, M. J. Charge-coupled device spectra of the Galilean satellites: molecular oxygen on Ganymede. *J. Geophys. Res.: Planets* **100**, 19049–19056 (1995).
- Hand, K. P., Chyba, C. F., Carlson, R. W. & Cooper, J. F. Clathrate hydrates of oxidants in the ice shell of Europa. *Astrobiology* **6**, 463–482 (2006).
- Plainaki, C. et al. The H<sub>2</sub>O and O<sub>2</sub> exospheres of Ganymede: the result of a complex interaction between the Jovian magnetospheric ions and the icy moon. *Icarus* **245**, 306–319 (2015).
- Johnson, R. E. et al. The origin and fate of O<sub>2</sub> in Europa's ice: an atmospheric perspective. *Space Sci. Rev.* **215**, 20 (2019).
- Plainaki, C. et al. Towards a global unified model of Europa's tenuous atmosphere. *Space Sci. Rev.* **214**, 40 (2018).
- Addison, P., Liuzzo, L. & Simon, S. Effect of the magnetospheric plasma interaction and solar illumination on ion sputtering of Europa's surface ice. *J. Geophys. Res.: Space Phys.* **127**, e2021JA030136 (2022).
- Szalay, J. et al. Oxygen production from dissociation of Europa's water-ice surface. *Nat. Astron.* **8**, 567–576 (2024).
- Van Cleeff, A. & Diepen, G. Gas hydrates of nitrogen and oxygen. *Recl. Trav. Chim. Pays-Bas* **79**, 582–586 (1960).
- Van Cleeff, A. & Diepen, G. Gas hydrates of nitrogen and oxygen. II. *Recl. Trav. Chim. Pays-Bas* **84**, 1085–1093 (1965).
- Holder, G., Zetts, S. & Pradhan, N. Phase behavior in systems containing clathrate hydrates: a review. *Rev. Chem. Eng.* **5**, 1–70 (1988).
- Loveday, J. & Nelmes, R. High-pressure gas hydrates. *Phys. Chem. Chem. Phys.* **10**, 937–950 (2008).
- Chou, I.-M. et al. Transformations in methane hydrates. *Proc. Natl Acad. Sci. USA* **97**, 13484–13487 (2000).
- Loveday, J. et al. Stable methane hydrate above 2 GPa and the source of Titan's atmospheric methane. *Nature* **410**, 661–663 (2001).
- Hirai, H. et al. Structural changes of argon hydrate under high pressure. *J. Phys. Chem. B* **106**, 11089–11092 (2002).
- Sasaki, S., Hori, S., Kume, T. & Shimizu, H. Microscopic observation and in-situ Raman scattering studies on high-pressure phase transformations of Kr hydrate. *J. Phys. Chem. B* **110**, 9838–9842 (2006).
- Loveday, J., Nelmes, R., Klug, D., Tse, J. & Desgreniers, S. Structural systematics in the clathrate hydrates under pressure. *Can. J. Phys.* **81**, 539–544 (2003).
- Tse, J., Handa, Y., Ratcliffe, C. & Powell, B. Structure of oxygen clathrate hydrate by neutron powder diffraction. *J. Incl. Phenom.* **4**, 235–240 (1986).
- Chazallon, B. & Kuhs, W. F. In situ structural properties of N<sub>2</sub>-, O<sub>2</sub>-, and air-clathrates by neutron diffraction. *J. Chem. Phys.* **117**, 308–320 (2002).
- Waite Jr, J. H. et al. Cassini ion and neutral mass spectrometer: Enceladus plume composition and structure. *Science* **311**, 1419–1422 (2006).
- Flasar, F. et al. Titan's atmospheric temperatures, winds, and composition. *Science* **308**, 975–978 (2005).
- Strobel, T. A., Sloan, E. D. & Koh, C. A. Raman spectroscopic studies of hydrogen clathrate hydrates. *J. Chem. Phys.* **130**, 014506 (2009).
- Kurnosov, A. V. et al. A new gas hydrate structure. *Dokl. Phys. Chem.* **381**, 303–305 (2001).
- Manakov, A. Y. et al. Structural investigations of argon hydrates at pressures up to 10 kbar. *J. Incl. Phenom. Macrocycl. Chem.* **48**, 11–18 (2004).
- Efimchenko, V. et al. New phase in the water–hydrogen system. *J. Alloy. Compd.* **509**, S860–S863 (2011).
- Amos, D. M. et al. A chiral gas–hydrate structure common to the carbon dioxide–water and hydrogen–water systems. *J. Phys. Chem. Lett.* **8**, 4295–4299 (2017).
- Catti, M. et al. Ne- and O<sub>2</sub>-filled ice XVII: a neutron diffraction study. *Phys. Chem. Chem. Phys.* **21**, 14671–14677 (2019).
- Loveday, J., Nelmes, R., Guthrie, M., Klug, D. & Tse, J. Transition from cage clathrate to filled ice: the structure of methane hydrate III. *Phys. Rev. Lett.* **87**, 215501 (2001).
- Bove, L. E. & Ranieri, U. Salt- and gas-filled ices under planetary conditions. *Philos. Trans. R. Soc. A* **377**, 20180262 (2019).
- Mishima, O., Calvert, L. & Whalley, E. 'Melting ice' I at 77 K and 10 kbar: a new method of making amorphous solids. *Nature* **310**, 393–395 (1984).
- Andersson, O., Brant Carvalho, P. H. B., Hsu, Y.-J. & Häussermann, U. Transitions in pressure-amorphized clathrate hydrates akin to those of amorphous ices. *J. Chem. Phys.* **151**, 014502 (2019).
- Yoshimura, Y., Stewart, S. T., Somayazulu, M., Mao, H.-K. & Hemley, R. J. High-pressure x-ray diffraction and Raman spectroscopy of ice VIII. *J. Chem. Phys.* **124**, 024502 (2006).
- Dyadin, Y. A., Aladko, E. Y. & Larionov, E. G. Decomposition of methane hydrates up to 15 kbar. *Mendelev Commun.* **7**, 34–35 (1997).
- Manakov, A. Y. et al. Argon hydrates: structural studies at high pressures. *Dokl. Phys. Chem.* **378**, 148–151 (2001).
- Dyadin, Y. A., Larionov, E., Aladko, E. Y. & Zhurko, F. Clathrate nitrogen hydrates at pressures of up to 15 kbar. *Dokl. Phys. Chem.* **378**, 159–161 (2001).
- Kuhs, W. F., Hansen, T. C. & Falenty, A. Filling ices with helium and the formation of helium clathrate hydrate. *J. Phys. Chem. Lett.* **9**, 3194–3198 (2018).
- Lokshin, K. A. et al. Structure and dynamics of hydrogen molecules in the novel clathrate hydrate by high pressure neutron diffraction. *Phys. Rev. Lett.* **93**, 125503 (2004).
- Kuzovnikov, M. & Tkacz, M. T–p–x phase diagram of the water–hydrogen system at pressures up to 10 kbar. *J. Phys. Chem. C* **123**, 3696–3702 (2019).
- Ranieri, U. et al. Observation of the most H<sub>2</sub>-dense filled ice under high pressure. *PNAS* **120**, e2312665120 (2023).
- Schaack, S. et al. Observation of methane filled hexagonal ice stable up to 150 GPa. *Proc. Natl Acad. Sci. USA* **116**, 16204–16209 (2019).
- Mehio, N., Dai, S. & Jiang, D.-e. Quantum mechanical basis for kinetic diameters of small gaseous molecules. *J. Phys. Chem. A* **118**, 1150–1154 (2014).

42. Abramson, E., Slutsky, L., Harrell, M. & Brown, J. Speed of sound and equation of state for fluid oxygen to 10 GPa. *J. Chem. Phys.* **110**, 10493–10497 (1999).
43. Mills, R., Liebenberg, D. & Bronson, J. Sound velocity and the equation of state of N<sub>2</sub> to 22 kbar. *J. Chem. Phys.* **63**, 1198–1204 (1975).
44. Carr, M. H. et al. Evidence for a subsurface ocean on Europa. *Nature* **391**, 363–365 (1998).
45. Kivelson, M., Khurana, K. & Volwerk, M. The permanent and inductive magnetic moments of Ganymede. *Icarus* **157**, 507–522 (2002).
46. Choblet, G., Tobie, G., Sotin, C., Kalousova, K. & Grasset, O. Heat transport in the high-pressure ice mantle of large icy moons. *Icarus* **285**, 252–262 (2017).
47. Melosh, H., Ekholm, A., Showman, A. & Lorenz, R. The temperature of Europa's subsurface water ocean. *Icarus* **168**, 498–502 (2004).
48. Fagents, S. A., Lopes, R. M., Quick, L. C. & Gregg, T. K. Cryovolcanism. In *Planetary Volcanism Across the Solar System* (eds Gregg, T. K. P., Lopes R. M. C. & Fagents, S. A.) 161–234 (Elsevier, 2022).
49. Sparks, W. B. et al. Active cryovolcanism on Europa? *Astrophys. J. Lett.* **839**, L18 (2017).
50. Showman, A. P., Mosqueira, I. & Head III, J. W. On the resurfacing of Ganymede by liquid–water volcanism. *Icarus* **172**, 625–640 (2004).
51. Nordheim, T., Hand, K. & Paranicas, C. Preservation of potential biosignatures in the shallow subsurface of Europa. *Nat. Astron.* **2**, 673–679 (2018).
52. Qin, Y., Dua, Q.-S., Xie, N.-Z., Li, J.-X. & Huang, R.-B. Exploring the possibility to store the mixed oxygen–hydrogen cluster in clathrate hydrate in molar ratio 1:2 (O<sub>2</sub> + 2H<sub>2</sub>). *J. Mol. Graph. Modell.* **73**, 1–7 (2017).
53. Billings, S. E. & Kattenhorn, S. A. The great thickness debate: Ice shell thickness models for Europa and comparisons with estimates based on flexure at ridges. *Icarus* **177**, 397–412 (2005).
54. Cockell, C. S. et al. Habitability: a review. *Astrobiology* **16**, 89–117 (2016).
55. Mao, H., Xu, J.-A. & Bell, P. Calibration of the ruby pressure gauge to 800 kbar under quasi-hydrostatic conditions. *J. Geophys. Res.: Solid Earth* **91**, 4673–4676 (1986).
56. Garbarino, G. et al. Extreme conditions x-ray diffraction and imaging beamline ID15B on the ESRF extremely brilliant source. *High Press. Res.* **44**, 199–216 (2024).
57. Anzellini, S. et al. Laser-heating system for high-pressure x-ray diffraction at the extreme conditions beamline I15 at Diamond light source. *J. Synchrotron Radiat.* **25**, 1860–1868 (2018).
58. Hirao, N. et al. New developments in high-pressure x-ray diffraction beamline for diamond anvil cell at SPring-8. *Matter Radiat. Extrem.* **5**, 018403 (2020).
59. Prescher, C. & Prakapenka, V. B. Dioptas: a program for reduction of two-dimensional x-ray diffraction data and data exploration. *High. Press. Res.* **35**, 223–230 (2015).
60. Rodríguez-Carvajal, J. Recent advances in magnetic structure determination by neutron powder diffraction. *Phys. B: Condens. Matter* **192**, 55–69 (1993).
61. Akahama, Y. & Kawamura, H. Raman spectroscopy on high-pressure fluids of molecular oxygen and nitrogen. *Chem. Phys. Lett.* **400**, 326–330 (2004).
62. Chou, I.-M., Blank, J. G., Goncharov, A. F., Mao, H.-k. & Hemley, R. J. In situ observations of a high-pressure phase of H<sub>2</sub>O ice. *Science* **281**, 809–812 (1998).

## Acknowledgements

M.F. acknowledges funding from the U.S. Department of Energy (DOE), Office of Fusion Energy Sciences funding numbers FWP100866 and FWP100182. The work was supported by the European Research Council (ERC) under the European Union's Horizon 2020 research and innovation programme (Grant agreement no. 948895, MetElOne). Sections of this work were carried out at Diamond Light Source I15. The XRD measurements at ID15b at ESRF were performed under proposal HC-5457. We acknowledge M. Hanfland, G. Garbarino, and S. Gallego-Parra for their beamline support. The XRD measurements at SPring-8 were performed at the BL10XU beamline with the approval of JASRI (2024A1404 and 2024A1415). We thank S. Kawaguchi for the beamline support.

## Author contributions

M.F., M.A.K., P.D.S., R.T.H., U.R., and E.G. performed experiments. E.G. conceived and designed the project. All authors analyzed data. J.S.L., M.A.K., and U.R. provided expertise on gas hydrates. M.F. wrote the first draft of the manuscript with input from all authors.

## Competing interests

The authors declare no competing interests.

## Additional information

**Supplementary information** The online version contains supplementary material available at <https://doi.org/10.1038/s42004-025-01509-y>.

**Correspondence** and requests for materials should be addressed to Mungo Frost or Eugene Gregoryanz.

**Peer review information** *Communications Chemistry* thanks the anonymous reviewers for their contribution to the peer review of this work. A peer reviewer report is available.

**Reprints and permissions information** is available at <http://www.nature.com/reprints>

**Publisher's note** Springer Nature remains neutral with regard to jurisdictional claims in published maps and institutional affiliations.

**Open Access** This article is licensed under a Creative Commons Attribution-NonCommercial-NoDerivatives 4.0 International License, which permits any non-commercial use, sharing, distribution and reproduction in any medium or format, as long as you give appropriate credit to the original author(s) and the source, provide a link to the Creative Commons licence, and indicate if you modified the licensed material. You do not have permission under this licence to share adapted material derived from this article or parts of it. The images or other third party material in this article are included in the article's Creative Commons licence, unless indicated otherwise in a credit line to the material. If material is not included in the article's Creative Commons licence and your intended use is not permitted by statutory regulation or exceeds the permitted use, you will need to obtain permission directly from the copyright holder. To view a copy of this licence, visit <http://creativecommons.org/licenses/by-nc-nd/4.0/>.

© The Author(s) 2025